Real space observation of spin frustration in Cr on a triangular lattice

M. Waśniowska,[1,*] S. Schröder,[2] P. Ferriani,[2] and S. Heinze[2]
[1]*Max-Planck-Institute of Microstructure Physics, Weinberg 2, D-06120 Halle, Germany*
[2]*Institut für Theoretische Physik und Astrophysik, Christian-Albrechts-Universität zu Kiel, 24098 Kiel, Germany*
(Received 1 February 2010; revised manuscript received 9 May 2010; published 2 July 2010)

Using spin-polarized scanning tunneling microscopy (SP-STM), we observe spin frustration in one monolayer Cr on the triangular lattice of the Pd(111) surface. Our STM measurements demonstrate pseudomorphic growth of the first Cr layer on Pd(111) without intermixing. Using SP-STM in the constant current mode, we observe three different types of images depending on the tip magnetization indicative of a noncollinear $(\sqrt{3}\times\sqrt{3})$ magnetic superstructure with an angle of 120° between moments of nearest-neighbor Cr atoms. The 120° Néel ground state of Cr/Pd(111) and the SP-STM images are explained based on our first-principles calculations.

DOI: 10.1103/PhysRevB.82.012402 PACS number(s): 75.70.Ak, 68.37.−d, 68.55.−a, 75.25.−j

The rich magnetic phase space of chromium has fascinated scientists for many years[1,2] and continues to challenge our theoretical understanding of itinerant magnetism. In its bulk bcc phase, Cr exhibits an intriguing antiferromagnetic spin-density wave due to Fermi-surface nesting. At the surface, the magnetic moments are enhanced and topological antiferromagnetism has been proposed for Cr(001),[3] i.e., antiferromagnetic coupling of adjacent layers with ferromagnetic (FM) alignment within each layer and experimentally confirmed.[4,5] Similarly, FM order within a monolayer (ML) of Cr on W(001) has been predicted[6] while recent experiments have reported local-antiferromagnetic order in a Cr monolayer on W(110) (Ref. 7) showing the crucial impact of surface orientation. On a triangular lattice or on a ferromagnetic surface, Cr nanostructures are a classical example of frustrated antiferromagnets. This triggered many theoretical studies reporting noncollinear magnetic ground states for clusters of a few atoms[8–10] or for ultrathin films.[11–13] While the absence of the Kondo effect in Cr trimers on Au(111) (Ref. 14) is consistent with this picture, no direct observation of spin frustration in such systems has so far been reported.

Here, we apply spin-polarized scanning tunneling microscopy (SP-STM) to prove the 120° Néel ground state of a Cr monolayer on the triangular lattice provided by the Pd(111) surface. Our STM measurements show pseudomorphic growth of the first Cr layer without intermixing. By using SP-STM we find three different types of images depending on the tip magnetization providing a real space observation of the noncollinear ground state. We find a reversal of the magnetic contrast due to switching of the tip's magnetization further proving the magnetic origin of the contrast. Our first-principles calculations confirm the Néel state of the Cr monolayer on Pd(111) due to a dominating antiferromagnetic nearest-neighbor exchange interaction. By simulating STM and SP-STM images we can explain the experimentally observed contrasts and obtain corrugation amplitudes in excellent agreement with the measured values.

In the classical Heisenberg model with only nearest-neighbor exchange interaction, an antiferromagnet on a triangular lattice exhibits a 120° Néel ground state, cf. Fig. 1(a). However, for itinerant antiferromagnets such as Cr, exchange interactions beyond nearest neighbors need to be considered. Depending on the relative sizes of first, second, and third nearest-neighbor exchange, the 120° Néel state, a collinear row-wise antiferromagnetic (RW-AFM) structure or a spin spiral can be energetically favorable, see Fig. 1(a). The exchange coupling in a monolayer film depends sensitively on the in-plane lattice constant as well as on the hybridization with the substrate. Therefore, an accurate description of the electronic structure is essential to determine the magnetic ground state of a specific system.

In order to gain insight into the magnetic properties of the Cr monolayer on Pd(111), we have performed first-principles calculations based on density-functional theory within the generalized-gradient approximation.[18] We applied the full-potential linearized augmented plane-wave method as implemented in the FLEUR code.[19,20] We used the theoretical lattice constant of Pd (a=3.891 Å) and considered a symmetric film including 7 ML Pd(111) and a Cr monolayer on each side to perform structural relaxations. We chose 72 k points in the irreducible part of the two-dimensional Brillouin zone (2D-BZ) and about 160 basis functions per atom. We found the Cr ML to be energetically more favorable in fcc than in hcp stacking by about 162 meV/Cr atom in the RW-AFM state. The fcc Cr ML in the RW-AFM state relaxes inward by 1.7% corresponding to an interlayer distance of 2.17 Å. For the spin-spiral calculations, the system has been modeled by an asymmetric film consisting of one Cr layer in fcc stacking on six layers of Pd(111) using the relaxed structure of the RW-AFM state. We used 1024 k points in the 2D-BZ and about 110 basis functions per atom.

We calculated the energy dispersion, $E(\mathbf{q})$, of flat spin spirals given by $M(\mathbf{R})=M[\cos(\mathbf{qR}),\sin(\mathbf{qR}),0]$, where M is the magnetic moment, $\mathbf{R}$ is a lattice vector, and $\mathbf{q}$ is the wave vector of the spin spiral. These structures are the general solution of the classical Heisenberg model on a periodic lattice allowing to explore a vast part of the magnetic phase space.[15] The energy dispersion for the unsupported ML (UML) of Cr on the in-plane lattice constant of Pd shown in Fig. 1(b) displays a global minimum at the $\bar{\mathrm{K}}$ point, corresponding to the Néel state, which is by about 39 meV/Cr atom lower than the RW-AFM state at $\bar{\mathrm{M}}$. For a Cr ML on the Pd(111) surface the dispersion curve is slightly modified, however, the ground state is still the Néel state which is by about 27 meV/atom lower than the RW-AFM state.[21] Due to hybridization with the substrate the magnetic moment of Cr decreases from $3.68\mu_B$ in the Cr UML to $3.21\mu_B$ on Pd(111).

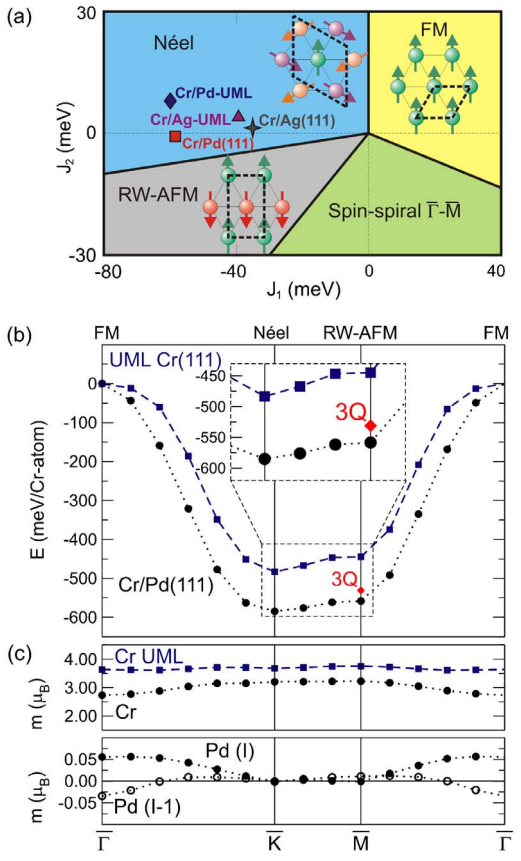

FIG. 1. (Color online) (a) J_1-J_2 phase diagram of the Heisenberg model on a triangular lattice at zero temperature. UMLs are characterized by a notation such as Cr/Ag UML, indicating a Cr UML on the lattice arrangement of Ag(111).(Ref. 15) Cr/Pd(111) and Cr/Ag(111) (Ref. 16) denotes the Cr ML on the substrate. (b) Calculated energy dispersion of spin spirals for Cr UMLs and on Cr/Pd(111). The $3Q$ denotes a superposition of spin spirals at the three equivalent $\bar{M}$ points of the 2D-BZ (Refs. 12 and 17). (c) Magnetic moments of the Cr atoms and of Pd atoms at the interface Pd(I) and one layer below Pd(I-1).

The induced moments in the Pd interface layer of the substrate are significant in the FM state, however, in the Néel state they vanish due to symmetry, cf. Fig. 1(c).

By fitting the energy dispersion to the classical Heisenberg model, we can obtain the exchange constants and interpret our first-principles calculations within the zero-temperature phase diagram.[20] As seen from Fig. 1(a), the nearest-neighbor exchange constant in the Cr ML on Pd(111) is large and negative (J_1=−58.4 meV), i.e., antiferromagnetic, and it clearly dominates over the second (J_2=−1.5 meV) and third nearest-neighbor (J_3=3.4 meV) exchange interaction. Compared to the UML of Cr the interactions beyond nearest neighbors are actually weakened while the nearest-neighbor exchange is nearly unaffected. In the J_1-J_2 phase diagram, the Cr ML is close to the axis J_2=0 meV due to dominating nearest-neighbor exchange. Enlarging the spacing between Cr atoms, e.g., by choosing the lattice constant of Ag(111) for both the Cr UML and Cr/Ag(111), lowers the antiferromagnetic nearest-neighbor exchange [cf. Fig. 1(a)].[15,16]

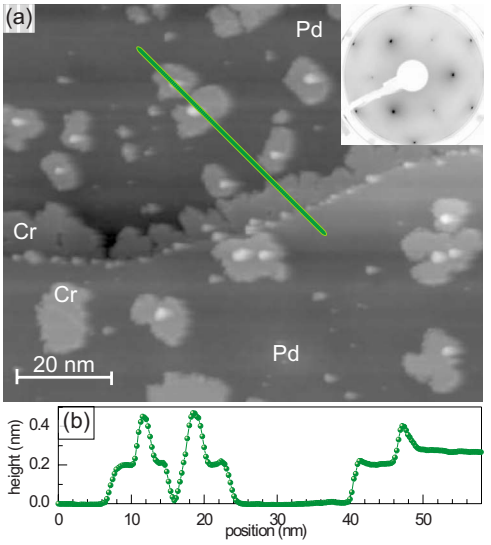

FIG. 2. (Color online) (a) Topography of the Pd(111) surface after deposition of 0.3-ML Cr at 200 K. The inset shows the LEED pattern of 0.3 ML Cr/Pd(111) surface at E=140 eV. The LEED pattern was taken at 200 K, immediately after deposition. (b) A line profile along the line in (a).

In order to verify the Néel ground state of Cr/Pd(111), we performed spin-polarized scanning tunneling microscopy experiments in an ultrahigh-vacuum (UHV) system with base pressure below 1×10^{-10} mbar. The Pd(111) single crystal was cleaned by sputtering at 300 K with Ar^+ ions followed by annealing to 870 K. Cr (99.999% purity) was deposited on Pd(111) by molecular-beam epitaxy at a sample temperature of 200 K and afterward the sample was immediately transferred to the STM to avoid possible intermixing between Cr and Pd atoms. We used chemically etched W tips cleaned by electron-beam heating in UHV chamber for atomic-resolution measurements. Magnetic tips were obtained by evaporating thick (≈50 ML) Cr layers on W tips, which are sensitive to an in-plane magnetization.[22] All STM images were taken in the constant current mode at 5 K.

Figure 2(a) shows an STM image of the topography for a submonolayer coverage of Cr deposited on Pd(111). At a temperature of 200 K, Cr grows as one layer high fcc islands with irregular shape.[23] On top of these islands the second Cr layer appears, moreover the substrate steps act as sinks for the Cr adatoms and some of the deposited material tends to decorate the lower step edges [cf. the line profile in Fig. 2(b)]. The low-energy electron-diffraction (LEED) measurements for the submonolayer coverage display a $p(1\times1)$ pattern without any additional structure around the spots indicating that the first layer of Cr is free from a dislocation network.

Atomically resolved STM images obtained with bare W tips also reveal the pseudomorphic arrangement of the Cr atoms in the monolayer and the images display a pattern corresponding to the chemical unit cell [Fig. 3(a)]. The distance between nearest-neighbor protrusions is 2.71 Å [cf. linescans in Fig. 3(e)], which corresponds well to the interatomic distance between Pd atoms in the single-crystal substrate. By comparison with the STM images obtained from

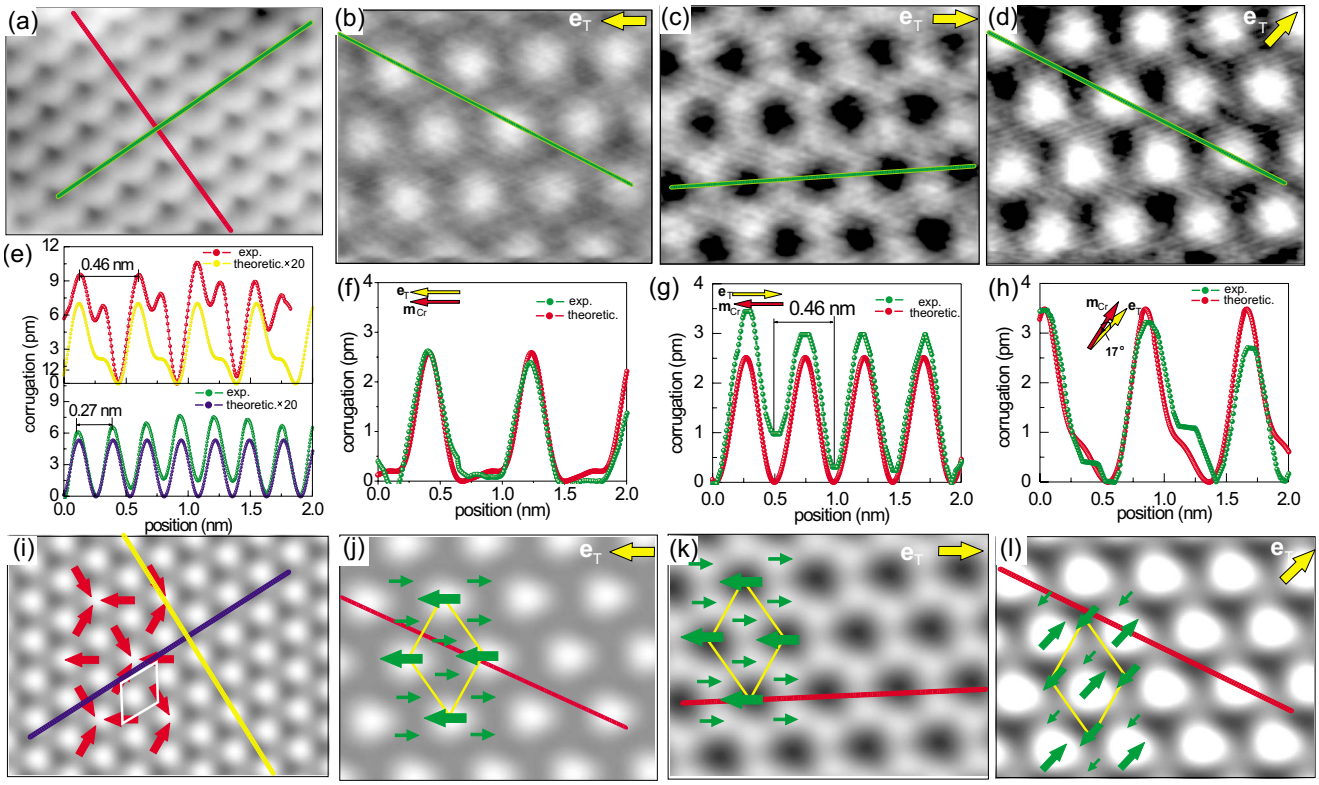

FIG. 3. (Color online) STM images of a Cr ML on Pd(111) obtained with (a) a bare W tip and [(b)–(d)] magnetic (Cr-coated W) tips with three different directions of the tip magnetization. The scan size is always about 2.0 nm × 1.7 nm and tunneling parameter: $U=14.1$ mV and $I=6.7$ nA. [(e)–(h)] Display line sections along the lines indicated in (a)–(d) and in comparison with the theoretical line sections obtained from (i)–(l) assuming a tip spin polarization of $P_T=0.18$ and a tip-sample distance of 4.2 Å (Ref. 24). Theoretical SP-STM images obtained from first-principles calculations based on the model of Ref. 16 are shown in (i)–(l). The 120° Néel state is indicated in (i) by red arrows representing the magnetic moments of the Cr atoms. In (j)–(k) the green arrows denote the projections $(\mathbf{e}_T\mathbf{m}_{\mathrm{Cr}})\mathbf{e}_T$ of the Cr moments (red arrows) $\mathbf{m}_{\mathrm{Cr}}$ onto the tip-magnetization direction (yellow arrows) $\mathbf{e}_T$. The chemical and magnetic unit cell is shown as a white and yellow rhombus, respectively.

our first-principles calculations based on the Tersoff-Hamann model,[24,25] Fig. 3(i), we can assign the observed protrusions to Cr atoms. Spin-polarized STM images obtained with various magnetically coated W tips display three qualitatively different contrasts seen in Figs. 3(b)–3(d). The images in Figs. 3(b) and 3(c) exhibit hexagonal patterns contrary to Fig. 3(d), which shows a threefold symmetry. However, these images are rotated by 30° with respect to the chemical unit cell and with a distance between protrusions of 0.46 nm [see line profiles in Fig. 3(f)], corresponding to a $\sqrt{3}\times\sqrt{3}$ unit cell with respect to the Pd(111) surface.[26] Similar SP-STM images have been obtained for a Mn ML on Ag(111) and interpreted as a Néel state.[27]

In our experiment, the Cr-coated W tips have an in-plane spin sensitivity but the in-plane direction remains undetermined and can change from one measurement to the other. An advantage of the variable magnetization direction of the tip is the possibility to observe different SP-STM contrasts of a spin structure. The obtained images can be explained based on the 120° Néel structure for the Cr monolayer, see arrows in Fig. 3(i). Depending on the magnetization direction of the tip, $\mathbf{e}_T$, and projections of the magnetic moments of the Cr atoms in the monolayer onto the tip-magnetization direction, three basic patterns are possible.[16,28] A hexagonal pattern as in Fig. 3(b) occurs if the tip magnetization is parallel to one of the Cr moments which appears as a protrusion and the projection onto the other two Cr moments is identical [see the arrows in Fig. 3(j)]. The observed SP-STM image is in excellent agreement with the theoretical one, Fig. 3(j), obtained from our first-principles calculations of Cr/Pd(111) using the spin-polarized Tersoff-Hamann model.[16] If the tip magnetization is antiparallel to one Cr moment, this pattern is simply inverted as observed experimentally in Fig. 3(c) and again in perfect agreement with the theoretical expectation, Fig. 3(k). Finally, if a tip magnetization is neither parallel nor antiparallel to one of the Cr moments, it leads to a pattern with a threefold contrast since the tip projection onto all Cr moments is different, as seen in Fig. 3(d).

We can even compare our calculations quantitatively with the experiment, by analyzing the line sections, Figs. 3(f)–3(h). As the tunneling parameters were identical for all SP-STM images, we expect a constant tip-sample distance. If we assume, e.g., a distance of 4.2 Å, we need to choose a tip spin polarization of $P_T=0.18$ to quantitatively reproduce all three line sections.[29] Moreover, the theoretical calculations allowed us to estimate the angle between the tip magnetization and one of the Cr atoms for the case of Fig. 3(d). The best fitting gives us an angle of 17°, which provides also a good agreement for the SP-STM images in Figs. 3(d) and 3(l).

Moreover, we sometimes observe a reversal of the contrast in the SP-STM images, which can be explained due to the switching of the magnetization of the tip's apex as seen from the sudden contrast inversion in the lower part of Fig. 4(a). In the upper part of the image, the tip's magnetization is antiparallel to the magnetic moment of one of the Cr atoms, which appear as depressions [cf. Fig. 3(c)]. However, in the lower part of the image the tip changes and the magnetization of the tip's apex is parallel to one of the Cr atoms. Therefore, the contrast appears inverted to the upper part of the image. The occurrence of a sudden switch of the tip's magnetization is also seen in the line section of Fig. 4(c) as well as multiply switching events in Figs. 4(b) and 4(d). Switching between these states could occur, e.g., due to magnetic exchange interaction between tip and sample[30] or due to the spin-polarized current.[31]

In summary, we investigated the magnetic and electronic properties for 1 ML Cr on Pd(111) by means of spin-averaged and spin-polarized scanning tunneling microscopy at 5 K. The results reveal that the initial film grows in three-dimensional irregular islands and the first layer grows pseudomorphically. Conventional STM measurements with nonmagnetic tips show the chemical unit cell containing three different contrast levels corresponding to the Cr atom and the fcc and hcp hollow site. Using spin-polarized STM operated in the constant current mode, we observe a $(\sqrt{3} \times \sqrt{3})$ superstructure indicative of a noncollinear magnetic ground state with moments forming 120° angles between nearest-neighbor Cr atoms, which is known as the Néel state.

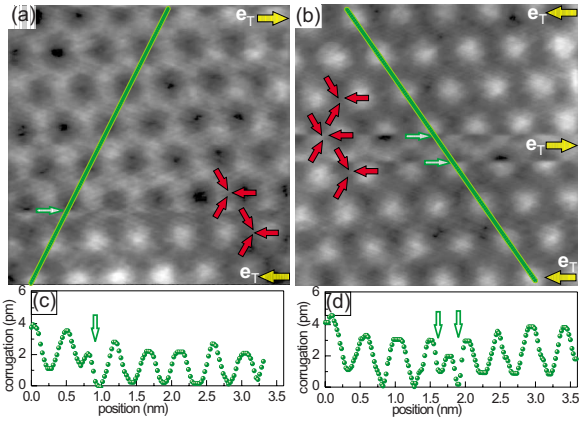

FIG. 4. (Color online) [(a) and (b)] SP-STM images of the Cr ML on Pd(111) showing a magnetic switching event of the Cr-coated W tips by the sudden inversion of the magnetic contrast. The scan size is 3 nm × 3 nm, tunneling parameters: $U=14.1$ mV and $I=7.7$ nA. The relative tip and Cr magnetizations are given by arrows. (b) and (c) show line profiles along the green lines in (a) and (b), respectively.

Our experimental observation are explained on the basis of the first-principles calculations.

We thank J. Kirschner for enabling the experiments and for insightful discussions. Financial support of the Stifterverband für die Deutsche Wissenschaft is gratefully acknowledged.

*Present address: Institute of Applied Physics, University of Hamburg, Jungiusstr. 11, D-20355 Hamburg, Germany.

[1] E. Fawcett, Rev. Mod. Phys. **60**, 209 (1988).
[2] H. Zabel, J. Phys.: Condens. Matter **11**, 9303 (1999).
[3] S. Blügel *et al.*, Phys. Rev. B **39**, 1392 (1989).
[4] R. Wiesendanger *et al.*, Phys. Rev. Lett. **65**, 247 (1990).
[5] M. Kleiber *et al.*, Phys. Rev. Lett. **85**, 4606 (2000).
[6] P. Ferriani *et al.*, Phys. Rev. B **72**, 024452 (2005).
[7] B. Santos *et al.*, New J. Phys. **10**, 013005 (2008).
[8] R. Robles and L. Nordström, Phys. Rev. B **74**, 094403 (2006).
[9] A. Bergman *et al.*, Phys. Rev. B **75**, 224425 (2007).
[10] A. Antal *et al.*, Phys. Rev. B **77**, 174429 (2008).
[11] D. Hobbs and J. Hafner, J. Phys.: Condens. Matter **12**, 7025 (2000).
[12] P. Kurz *et al.*, J. Appl. Phys. **87**, 6101 (2000).
[13] R. Robles *et al.*, Phys. Rev. B **68**, 094413 (2003).
[14] T. Jamneala *et al.*, Phys. Rev. Lett. **87**, 256804 (2001).
[15] P. Kurz, Ph.D. thesis, RWTH Aachen, 2000.
[16] D. Wortmann *et al.*, Phys. Rev. Lett. **86**, 4132 (2001).
[17] Spin interactions beyond Heisenberg exchange can lower the energy of multi-Q states such as the $3Q$ state (Ref. 12) with respect to spin spirals. However, in our calculation the total energy of the $3Q$ states is higher by about 24 meV/Cr atom than the RW-AFM state and the Néel state remains the lowest state.
[18] Y. Zhang and W. Yang, Phys. Rev. Lett. **80**, 890 (1998).
[19] www.flapw.de
[20] Ph. Kurz *et al.*, Phys. Rev. B **69**, 024415 (2004).
[21] Using the local-density approximation we find an energy difference of 55 meV/Cr atom in favor of the Néel state.
[22] A. Wachowiak, J. Wiebe, M. Bode, O. Pietzsch, M. Morgenstern, and R. Wiesendanger, Science **298**, 577 (2002).
[23] We have performed spectroscopy measurements on Cr islands and on Cr stripes grown at the step edges. The spectra are of very similar shape with peaks located at the same positions. As the fcc stacking of the substrate is continued by Cr growing at the step edges, we conclude fcc stacking also for the Cr islands. These observations are supported by our calculations, which demonstrate that hcp stacking of Cr is energetically very unfavorable by 162 meV/Cr atom.
[24] A discrepancy of a factor 20 compared to the experiment for the corrugation amplitude for the nonmagnetic image is a well-known deficiency of the Tersoff-Hamann model (Ref. 25) for close-packed metal surfaces.
[25] J. Tersoff and D. R. Hamann, Phys. Rev. B **31**, 805 (1985).
[26] We exclude alloy formation due to intermixing between Cr and Pd atoms as the sample was prepared at low temperature and in atomically resolved STM images with W tips a $p(1\times1)$ cell was always observed.
[27] C. L. Gao *et al.*, Phys. Rev. Lett. **101**, 267205 (2008).
[28] S. Heinze *et al.*, Appl. Phys. A: Mater. Sci. Process. **75**, 25 (2002).
[29] From our fits we find that the spin polarization does not change significantly with the voltage for small biases between −50 and +50 mV while it increases to about 0.4 by assuming a tip-sample distance of 5 Å.
[30] R. Schmidt *et al.*, Nano Lett. **9**, 200 (2009).
[31] S. Krause *et al.*, Science **317**, 1537 (2007).